

Direct X-Ray Measurements of Strain in Monolayer MoS₂ from Capping Layers and Geometrical Features

Kathryn Neilson¹, Marc Jaikissoon¹, Dante Zakhidov², Tara Peña¹, Alberto Salleo², Krishna Saraswat^{1,2}, and Eric Pop^{1,2,3,*}

¹ *Department of Electrical Engineering, Stanford University, Stanford, CA 94305*

² *Department of Materials Science and Engineering, Stanford University, Stanford, CA 94305*

³ *Department of Applied Physics, Stanford University, Stanford, CA 94305*

*Contact: epop@stanford.edu

ABSTRACT: Strain induced through fabrication, both by patterning and capping, can be used to change the properties of two-dimensional (2D) materials or other thin films. Here, we explore how capping layers impart strain to monolayer MoS₂ using direct x-ray diffraction measurements of the lattice. We first observe the impact of naturally-oxidized metal layers (~1.5 nm Al) and subsequently-deposited Al₂O₃ (15 nm to 25 nm thick) on the 2D material, and find that the strain imparted to MoS₂ is mainly controlled by the interfacial adhesion of the seed layer in addition to the substrate adhesion. Then, using test structures which mimic transistor contacts, we measure enhanced strain from such patterns compared to blanket films. Furthermore, we observe significant tensile strain—up to 2% in monolayer MoS₂, one of the largest experimental values to date on a rigid substrate—due to highly-stressed blanket metal capping layers. These results provide direct evidence supporting previous reports of strain effects in 2D material devices.

Atomically thin two-dimensional (2D) materials have gained much attention since monolayer graphene was isolated and electrically probed¹ in 2004. In particular, the sub-nanometer thickness of 2D semiconductor monolayers (the most common being transition metal dichalcogenides, or TMDs) makes them ideal for transistor scaling.² When integrating such materials on various substrates, strain is often present, either from the high-temperature synthesis process or from subsequent fabrication steps, contacts, or capping layers.³⁻⁷ Even small amounts of strain (~1%) can be used in a wide variety of applications, including (but not limited to) band gap tuning,^{8,9} phase transformations,¹⁰⁻¹² inducing novel quantum states,¹³ and in conventional silicon technology.¹⁴ Strain engineering can therefore provide an opportunity to enhance properties of 2D materials by changing their band structure and associated properties.

Recent studies^{5,15-20} have found that tensile strain applied to monolayer (1L) TMDs increases the energy separation between the (lower) conduction band K valley and (upper) Q valley, decreasing the intervalley scattering of electrons and increasing their mobility. A similar principle is emerging for the valence band

of TMDs, although the performance benefit is reported to arise with compressive strain^{21,22} due to the increased valley separation in the valence band.²³ To estimate the strain, reports^{24,25} have used indirect optical methods like photoluminescence and Raman spectroscopy. However, the analysis of the data obtained with these techniques can lead to inaccurate strain estimates because the materials' response must be calibrated separately and is also affected by dopants, defects, and the environment.²⁶ The most *direct* approach is to measure the lattice spacing of the crystal, and hence strain, by x-ray diffraction (XRD), the gold standard in structural materials characterization. An additional benefit of XRD over techniques such as photoluminescence and Raman is that XRD measures a larger area, and that XRD can measure through thicker metal.

In this work, we use XRD to directly measure the strain imparted in monolayer MoS₂ from its synthesis (on SiO₂/Si), from capping with common uniform layers (e.g. AlO_x), and from parallel metal lines which mimic transistor-like geometries. We find that the atomic layer deposition (ALD) temperature²⁷ and thickness of the AlO_x capping has little impact on the strain imparted to the underlying 2D film. Nevertheless, we observe a small strain (~0.1%), which is mainly due to the seed layer used for ALD nucleation. The strain of the monolayer MoS₂ however is increased by ~6 times when Au metal lines capped by AlO_x are used instead, due to the geometry effect on strain distribution. Finally, we use a highly strained blanket capping layer of Au/Ti/Ni on transferred MoS₂ and achieve a measured tensile strain of ~2%, demonstrating potential tunability in the band structure of monolayer 2D materials on rigid, rather than flexible, substrates.

Monolayer MoS₂ is grown at 750 °C on 90 nm SiO₂ on Si substrates using perylene-3,4,9,10-tetracarboxylic acid tetrapotassium salt (PTAS) as growth promoter²⁸. Samples are carefully selected for large-area coverage and 50-100 μm grain size [shown in **Fig. 1(a)**]. Most MoS₂ films were examined as-grown, but a few were also examined after transfer to a new SiO₂/Si substrate. If transferred, MoS₂ chips are coated with a polystyrene/toluene mix (3 g/20 mL), delaminating the MoS₂ in water, and finally picking up the MoS₂/polymer with a target substrate. The polymer is subsequently removed in solvent, and a further anneal (250 °C, 2 hrs, in ~10⁻⁶ Torr) is implemented to better adhere the MoS₂ to the substrate. Then, capping layers were deposited as blanket films onto MoS₂ with and without patterning and metallization.

Grazing incidence x-ray diffraction (GIXRD) is carried out on beamline 10-2a at SLAC National Accelerator Lab [**Fig. 1(b)**], using a 14 keV source ($\lambda = 0.8856 \text{ \AA}$). A 3D-printed PET (polyethylene terephthalate) holder clasps samples at a 90° angle through a vacuum attachment at the back of the holder, and Pb foil shields are placed at the front of the holder, nearest to the incident beam, to prevent additional background scattering from the polymer [**Fig. 1(c)**]. Finally, the holder is covered in x-ray transparent thermal tape and filled with N₂ ambient gas to reduce noise from air scattering and mitigate beam damage. Incident x-rays enter through the side of the PET holder, diffract off the MoS₂ chip, are filtered through Soller slits, and finally absorbed by the detector, as shown in **Fig. 1(d)**.

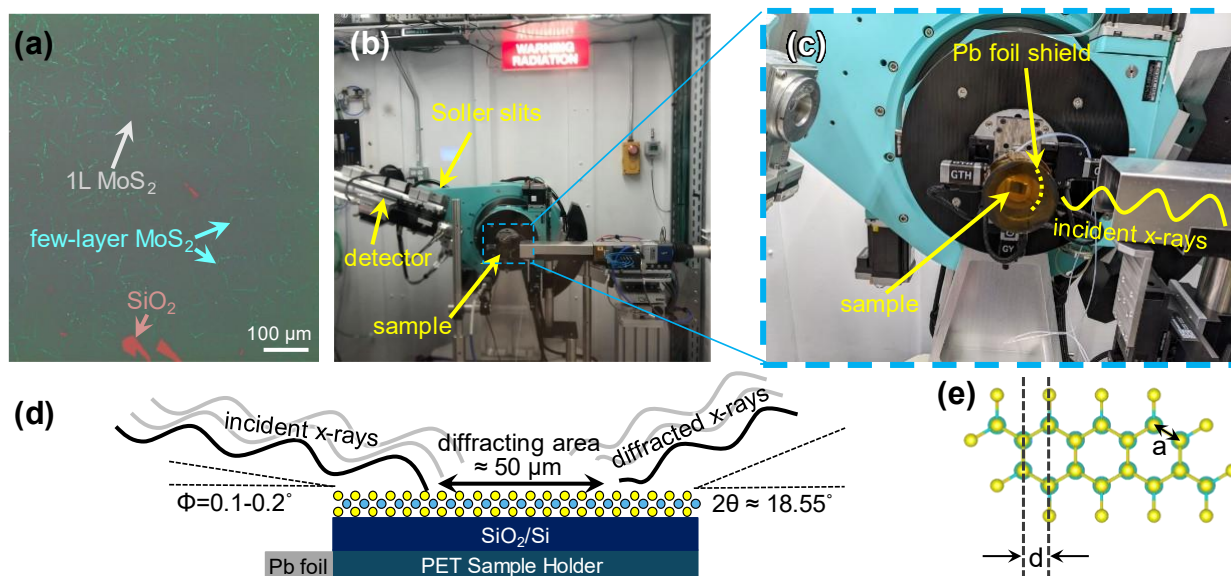


FIG. 1. (a) Optical image of coalesced monolayer (1L) MoS₂ with few-layer regions along the grain edges. (b) Hutch station for grazing incidence x-ray diffraction (GIXRD), where x-rays are incident from the right side of the image, diffract off the sample, are filtered through the Soller slits, and finally absorbed by the detector. (c) Close-up image of the GIXRD setup, including a Pb foil shield which helps absorb scattered x-rays from the polymer sample holder. The holder is sealed with thermal tape and filled with N₂ gas. (d) Schematic of the GIXRD scattering process. The grazing incident angle is 0.1-0.2° (depending on the sample), corresponding to a ~50 μm diffraction spot size. (e) Top-down view of monolayer MoS₂ crystal structure. The x-ray probes the $d = \sqrt{3}a/2$ spacing, where a is the lattice constant. We measure the in-plane lattice spacing to evaluate strain as relevant for charge transport.

X-rays diffract off the MoS₂ lattice according to Bragg's Law, $n\lambda = 2d \sin(\theta)$, where n is a positive integer, λ is the incident x-ray wavelength, d is the spacing labeled in **Fig. 1(e)**, and θ is the diffracted angle. For 2D materials, we measure the (01) peak to directly evaluate in-plane strain, which is of interest to examine how capping layers⁵ and metal contacts⁶ may affect planar transistors. Resulting diffraction peak positions and the corresponding d spacing for all spectra in this study are found in **Tables S1-S6**.

First, we measured the as-grown strain in monolayer MoS₂ by comparing as-grown materials with films transferred onto a bare 90 nm SiO₂ on Si chip. From **Fig. 2(a)**, it is confirmed that the as-grown monolayer MoS₂ tends to have built-in tensile strain,^{3,29} here ~0.5% for CVD growth at 750 °C. After the layer transfer onto a new SiO₂/Si substrate, the built-in strain is released, and some compressive strain may be introduced, depending on the transfer method. Tensile strain in the as-grown MoS₂ arises due to a mismatch between the coefficient of thermal expansion (CTE) of the SiO₂ substrate and the 2D material during the cool-down process after growth. Transferred MoS₂ will have lower adhesion to the substrate, relying on the weak van der Waals interaction of the 2D material and the SiO₂ underneath.^{4,30}

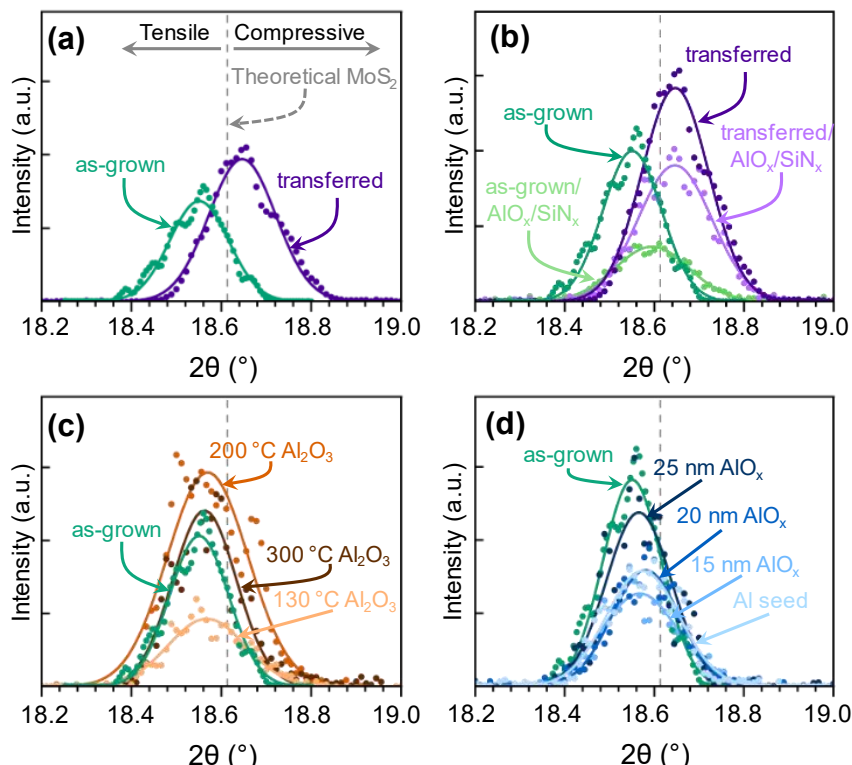


FIG. 2. (a) GIXRD comparing as-grown monolayer MoS₂ vs. transferred MoS₂ onto the same substrate, 90 nm SiO₂ on silicon. The built-in tensile strain (ϵ) from thermal expansion mismatch during growth is released upon transfer. Symbols represent experimental data, lines are Gaussian fits. The change in strain compared to theoretical lattice spacing is $\epsilon = 0.33\%$ for as-grown, and -0.18% for transferred MoS₂. (b) Comparing the strain imparted into MoS₂ (using ~ 1.5 nm Al seed layer, followed by 5 nm Al₂O₃ and 15 nm SiN_x) on an as-grown MoS₂ sample and a transferred MoS₂ sample. The transferred sample sees no change in the diffraction angle, while the as-grown sees a shift to less tensile strain, indicating that the adhesion to the substrate plays a critical role in strain transfer. The change in strain with the additional alumina and silicon nitride layers is $\epsilon = -0.23\%$ for as-grown, and 0% for transferred MoS₂. (c) Comparing the effect of deposition temperature of ALD alumina (~ 15 nm thick) on the strain it imparts into monolayer MoS₂. All peaks show a similar center position, indicating that the ALD deposition temperature has little impact on strain imparted into MoS₂. The change in strain with increasing temperature follows as $\epsilon = -0.08, -0.09, -0.06\%$. (d) Varying the thickness of alumina to test how the ALD encapsulation changes strain in MoS₂. All samples start with 1.5 nm Al seed, followed by subsequent ALD at 130 °C; all peaks show a similarly small right-shift to higher angles, as the Al seed at the 2D interface plays the biggest role. The change in strain with increasing thickness follows as $\epsilon = -0.12, -0.08, -0.15\%$, and -0.07% for Al seed, 15 nm, 20 nm, and 25 nm of alumina, respectively. All diffraction peaks shown are the (01) peak of MoS₂. Details for strain calculations can be found in **Tables S1-S4** for (a)-(d), respectively.

Another experiment is shown in **Fig. 2(b)**, where a capping layer consisting of ~ 1.5 nm Al seed with 5 nm ALD Al₂O₃ and 15 nm SiN_x transfers significant compressive strain (-0.23%) to an as-grown MoS₂ film (indicated by the higher angle of the diffraction peak), but the same amount of compressive strain is not imparted in MoS₂ transferred onto a new substrate, revealing the importance of substrate adhesion in strain transfer.³¹ This has important implications for engineering the strain, as the adhesion to the substrate must also be optimized, in addition to the in-plane stresses to obtain the desired change in band structure.

ALD films are commonly deposited onto 2D materials for a variety of purposes, including doping,³² capping,³³ and top-gate dielectrics;^{34,35} therefore, it is important to understand if, and how, they affect the 2D material strain. Because the ALD process requires attachment to partially filled dangling bonds, seed layers (such Al or Si, which then oxidize³⁴) are often deposited in sub-2 nm thickness to provide a template for further oxide film growth. In **Fig. 2(c)** we find that ALD alumina at different temperatures²⁷ does not lead to different amounts of strain; rather, the imparted strain (-0.1%) is due to the initially evaporated seed layer. Increasing alumina thickness does not impart additional strain either [**Fig. 2(d)**], suggesting that ALD of oxide films may not be the most effective approach for intentionally straining 2D material devices, as amorphous films are more able to easily re-coordinate and relax strain in the system.

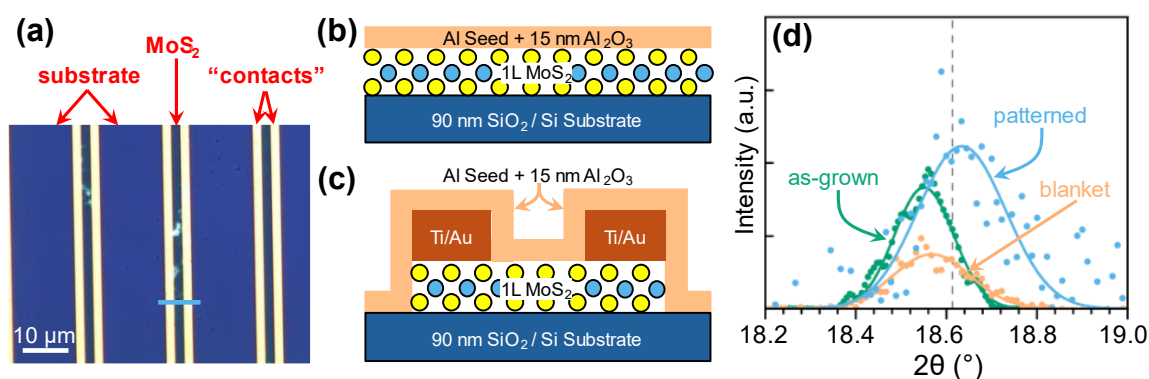


Fig. 3. (a) Top-down optical image of the test structure for GIXRD measurements of patterned samples. Long strips of MoS₂ with metal contacts on either side (5 nm Ti/ 45 nm Au) serve as an analog to a conventional transistor. The x-ray beam passes parallel to the metal contacts during measurement. The entire sample is covered with Al seed and 15 nm ALD Al₂O₃. (b) Cross-section schematic of blanket alumina-capped MoS₂ films shown in the XRD spectra, and (c) patterned alumina-capped MoS₂, across the blue line shown in (a). (d) Comparing GIXRD spectra of MoS₂ films that are as-grown (not capped), blanket-capped as in (b), and patterned then capped as in (a) and (c). The patterned sample sees a greater shift to higher angles, indicating a larger quantity of strain (here, approximately -0.44%) due to geometry as opposed to the blanket films (-0.08%). Calculation and fitting details can be found in supplementary material **Table S5**.

Thus far, we have examined strain imparted into MoS₂ by blanket capping layers; however, it is important to study the strain for different geometries of the capping layer, as strain can depend on the dimensions of the film stressor and/or the presence of metal contacts and gates (i.e. transistor topography). In **Fig. 3(a)** we pattern the MoS₂ into strips with long metal “contact” lines, to mimic a transistor-like geometry, keeping in mind that individual devices (with sub-micron dimensions) would not yield sufficient GIXRD signal-to-noise. **Figures 3(b)** and **3(c)** display cross-sections of the control sample (with only alumina blanket film) and the patterned transistor-like sample (with metal line contacts and alumina capping). Au is chosen as the contact, as Au metal lines alone impart minimal strain into the 2D material.²⁶ The GIXRD results are shown in **Fig. 3(d)**, revealing that the samples with patterned contact lines display ~6× greater strain (-0.44% vs. -0.07%) compared to samples with blanket ALD Al₂O₃, giving direct evidence that the geometry can

further enhance strain transfer in transistors. We note that the patterned sample has a larger full width at half maximum due to non-uniform strain that is known to occur along the device channel.^{6,36,37}

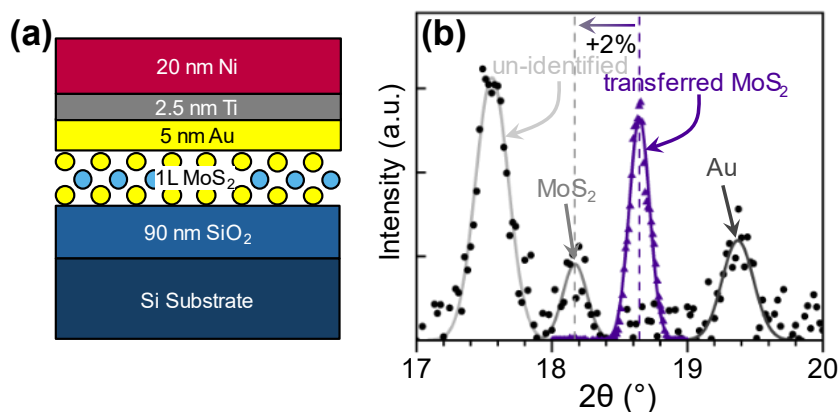


FIG. 4. (a) Schematic of a high-strain blanket metal capping layer on monolayer MoS₂, similar to the stacks used in Jaikissoo *et al.*⁶ Here the MoS₂ is transferred, not directly grown, on this SiO₂/Si substrate. **(b)** Measured x-ray spectra for the MoS₂ (purple symbols, without capping) and after the high-stress capping layer (black symbols and line fits). Three peaks are visible for the metal-capped sample: one from Au, one assigned to the 1H MoS₂, and a left-most peak that cannot be assigned. Compared to the uncapped, transferred MoS₂, this metal-capped stack shows large tensile strain (>2%) imparted into the 2D material. Parameters for the stress calculation can be found in supplementary material **Table S6**.

To utilize the excess strain that can be imparted through geometry, we have previously shown that materials like Ni can be deposited on the contact region, imparting strain to the MoS₂ channel and increasing the short-channel device current.⁶ Here we use a similar metal stack, illustrated in **Fig. 4(a)**, to study the strain it can impart as a blanket capping layer on MoS₂. The stack consists of monolayer MoS₂ capped with 5 nm Au, 2.5 nm Ti as a sticking layer, and 20 nm Ni as stressor. **Figure 4(b)** displays the resulting XRD spectra, showing tensile strain on the order of 2% imparted to the MoS₂, which is a substantial amount given that typical reports give values on the range of 0.5-1%. To our knowledge, this is the one of the largest magnitudes of strain to date reported on a rigid substrate imparted into a monolayer 2D material. Factors such as adhesion to the substrate, geometry from patterning, and potential cracking of the material under too high of a strain could all play a role in local strain relaxation. However, there are a few distinctions to our findings, which require additional discussion.

First, most reports of large strains have been estimated with Raman spectroscopy, which gives less accurate results (due to doping or plasmon coupling effects) and is unable to probe through thicker metal layers.²⁶ And second, we observe a diffraction peak at the smallest angle (~17.6°) in the metal-capped sample. While this peak cannot be confidently attributed to a particular phase (**Table S7** lists possible phases and their corresponding *d* spacing), the closest intermetallic to our knowledge is metastable TiAu, formed by ion irradiation. This peak could also be due to strain non-uniformity, as previously suggested.³⁷ Alternatively,

if large strains are present, there could be localized areas where highly-strained 1T' MoS₂ is present. Theoretical analysis of the 1H to 1T' transition^{38,39} has suggested that a phase transformation could occur with large amounts of tensile strain, greater than 10% for biaxially strained MoS₂. However, factors such as mixed phase forms of 2D materials, phonon vibrations, and salt incorporation (i.e. the potassium from PTAS) from the growth may decrease the amount of strain for a phase transformation.^{40,41} We note that contact electrodes on 2D materials with this metal stack (Au/Ti/Ni) are unlikely to fully benefit from such large strains, because the strain profile in the MoS₂ changes rapidly under the contact (within 10s of nm),³⁶ unlike the blanket case presented here.

In summary, we used grazing-incidence x-ray diffraction to directly measure the strain imparted in monolayer MoS₂ by common capping layers (AlO_x, SiN_x), contact metals (Ni), as blanket layers and in transistor-like contact geometries. We find that strain imparted from Al₂O₃ by ALD is controlled by the Al seed layer deposited on the 2D material, and not by the Al₂O₃ thickness or ALD temperature. We also found that long metal lines deposited on MoS₂, which mimic transistor contacts, can provide ~6 times higher strain compared to blanket Al₂O₃ layers. Blanket metal stacks with stressed Ni can impart even greater strain in MoS₂, up to 2%. Further data analysis of diffraction line shapes may provide more information on the uniformity of the strain. These x-ray measurements directly probe the (average) lattice spacing, providing valuable insight into tuning the band structure of monolayer 2D materials using insulating and metal capping layers.

This work was performed in part at the Stanford Nanofabrication Facility (SNF) and Stanford Nano Shared Facilities (SNSF), RRID:SCR_023230, supported by the National Science Foundation (NSF) under Award ECCS-2026822. K.N. acknowledges the Stanford Graduate Fellowship (SGF) program, and K.N. and D.Z. acknowledges the NSF Graduate Research Fellowship under Grant No. DGE-1656518. Synchrotron measurements were done at the SLAC National Accelerator Laboratory, supported by the Department of Energy under Contract No. DE-AC02-76-SF0015. The work was supported in part by the Stanford SystemX Alliance. K.N. and E.P. acknowledge partial support by Intel Corp. and NSF FuSe2 Award 2425218, M.J. and K.S. acknowledge the Samsung Global Research Outreach (GRO) program.

AUTHOR DECLARATIONS

Conflict of Interest

The authors have no conflicts to disclose.

Acknowledgements

The authors would like to thank Dr. Christopher Takacs from SLAC for his assistance on the beamline.

Contributions

K.N. and D.Z. performed the GIXRD measurements. M.J. synthesized the MoS₂. K.N. did associated patterning of MoS₂ samples, and K.N. and M.J. deposited films onto MoS₂. All authors assisted with the preparation of the manuscript. A.S., K.S., and E.P. supervised the project.

DATA AVAILABILITY

The data supporting this study are available from the corresponding author upon reasonable request.

References

- 1 K.S. Novoselov, A.K. Geim, S.V. Morozov, D. Jiang, Y. Zhang, S.V. Dubonos, I.V. Grigorieva, and A.A. Firsov, *Science* **306** (5696), 666 (2004).
- 2 K.P. O'Brien, C.H. Naylor, C. Dorow, K. Maxey, A.V. Penumatcha, A. Vyatskikh, T. Zhong, A. Kitamura, S. Lee, C. Rogan, W. Mortelmans, M.S. Kavrik, R. Steinhardt, P. Buragohain, S. Dutta, T. Tronic, S. Clendenning, P. Fischer, E.S. Putna, M. Radosavljevic, M. Metz, and U. Avci, *Nature Communications* **14** (1), 6400 (2023).
- 3 G.H. Ahn, M. Amani, H. Rasool, D.-H. Lien, J.P. Mastandrea, J.W. Ager III, M. Dubey, D.C. Chrzan, A.M. Minor, and A. Javey, *Nature Communications* **8** (1), 608 (2017).
- 4 Y. Zhang, M.A. Hossain, K.J. Hwang, P.F. Ferrari, J. Maduzia, T. Peña, S.M. Wu, E. Ertekin, and A.M. van der Zande, *ACS Nano* **18** (5), 4205 (2024).
- 5 T. Peña, S.A. Chowdhury, A. Azizimanesh, A. Sewaket, H. Askari, and S.M. Wu, *2D Materials* **8** (4), 045001 (2021).
- 6 M. Jaikissoon, E. Pop, and K.C. Saraswat, *IEEE Electron Device Letters* **45** (8), 1528 (2024).
- 7 M. Jaikissoon, Ç. Koroğlu, J.A. Yang, K. Neilson, K.C. Saraswat, and E. Pop, *Nature Electronics* **7** (10), 885 (2024).
- 8 S. Manzeli, A. Allain, A. Ghadimi, and A. Kis, *Nano Letters* **15** (8), 5330 (2015).
- 9 R. Schmidt, I. Niehues, R. Schneider, M. Drüppel, T. Deilmann, M. Rohlffing, S.M. de Vasconcellos, A. Castellanos-Gomez, and R. Bratschitsch, *2D Materials* **3** (2), 021011 (2016).
- 10 E. Scalise, M. Houssa, G. Pourtois, V. Afanas'ev, and A. Stesmans, *Nano Research* **5** (1), 43 (2012).
- 11 M. Kan, B. Wang, Y.H. Lee, and Q. Sun, *Nano Research* **8** (4), 1348 (2015).
- 12 X. Xu, S. Chen, S. Liu, X. Cheng, W. Xu, P. Li, Y. Wan, S. Yang, W. Gong, K. Yuan, P. Gao, Y. Ye, and L. Dai, *Journal of the American Chemical Society* **141** (5), 2128 (2019).
- 13 F. Guinea, M.I. Katsnelson, and A.K. Geim, *Nature Physics* **6** (1), 30 (2010).
- 14 S.E. Thompson, M. Armstrong, C. Auth, M. Alavi, M. Buehler, R. Chau, S. Cea, T. Ghani, G. Glass, T. Hoffman, C.H. Jan, C. Kenyon, J. Klaus, K. Kuhn, M. Zhiyong, B. Mcintyre, K. Mistry, A. Murthy, B. Obradovic, R. Nagisetty, N. Phi, S. Sivakumar, R. Shaheed, L. Shifren, B. Tufts, S. Tyagi, M. Bohr, and Y. El-Mansy, *IEEE Transactions on Electron Devices* **51** (11), 1790 (2004).
- 15 I.M. Datye, A. Daus, R.W. Grady, K. Brenner, S. Vaziri, and E. Pop, *Nano Letters* **22** (20), 8052 (2022).
- 16 Y. Zhang, H.L. Zhao, S. Huang, M.A. Hossain, and A.M. van der Zande, *ACS Nano* **18** (19), 12377 (2024).
- 17 J.A. Yang, R.K.A. Bennett, L. Hoang, Z. Zhang, K.J. Thompson, A. Michail, J. Parthenios, K. Papagelis, A.J. Mannix, and E. Pop, *ACS Nano* **18** (28), 18151 (2024).
- 18 X. Liu, B. Erbas, A. Conde-Rubio, N. Rivano, Z. Wang, J. Jiang, S. Bienz, N. Kumar, T. Sohler, M. Penedo, M. Banerjee, G. Fantner, R. Zenobi, N. Marzari, A. Kis, G. Boero, and J. Brugger, *Nature Communications* **15** (1), 6934 (2024).
- 19 M. Hosseini, M. Elahi, M. Pourfath, and D. Esseni, *IEEE Transactions on Electron Devices* **62** (10), 3192 (2015).
- 20 M. Hosseini, M. Elahi, M. Pourfath, and D. Esseni, *Journal of Physics D: Applied Physics* **48** (37), 375104 (2015).

- 21 A. Oberoi, Y. Han, S.P. Stepanoff, A. Pannone, Y. Sun, Y.-C. Lin, C. Chen, J.R. Shallenberger,
D. Zhou, M. Terrones, J.M. Redwing, J.A. Robinson, D.E. Wolfe, Y. Yang, and S. Das, *ACS*
Nano **17** (20), 19709 (2023).
- 22 M.A. Islam, E. Nicholson, N. Barri, M. Onodera, D. Starkov, P. Serles, S. He, B. Kumral, A.
Zavabeti, H. Shahsa, T. Cui, G. Wang, T. Machida, C.V. Singh, and T. Filleter, *Advanced*
Electronic Materials **n/a** (n/a), 2400225 (2024).
- 23 B. Amin, T.P. Kaloni, and U. Schwingenschlögl, *RSC Advances* **4** (65), 34561 (2014).
- 24 D. Lloyd, X. Liu, J.W. Christopher, L. Cantley, A. Wadehra, B.L. Kim, B.B. Goldberg, A.K.
Swan, and J.S. Bunch, *Nano Letters* **16** (9), 5836 (2016).
- 25 A. Michail, D. Anastopoulos, N. Delikoukos, S. Grammatikopoulos, S.A. Tsirkas, N.N.
Lathiotakis, O. Frank, K. Filintoglou, J. Parthenios, and K. Papagelis, *The Journal of Physical*
Chemistry C **127** (7), 3506 (2023).
- 26 K. Schauble, D. Zakhidov, E. Yalon, S. Deshmukh, R.W. Grady, K.A. Cooley, C.J. McClellan, S.
Vaziri, D. Passarello, S.E. Mohny, M.F. Toney, A.K. Sood, A. Salleo, and E. Pop, *ACS Nano*
14 (11), 14798 (2020).
- 27 O.M.E. Ylivaara, X. Liu, L. Kilpi, J. Lyytinen, D. Schneider, M. Laitinen, J. Julin, S. Ali, S.
Sintonen, M. Berdova, E. Haimi, T. Sajavaara, H. Ronkainen, H. Lipsanen, J. Koskinen, S.-P.
Hannula, and R.L. Puurunen, *Thin Solid Films* **552**, 124 (2014).
- 28 K.K.H. Smithe, S.V. Suryavanshi, M. Muñoz Rojo, A.D. Tedjarati, and E. Pop, *ACS Nano* **11**
(8), 8456 (2017).
- 29 W.H. Chae, J.D. Cain, E.D. Hanson, A.A. Murthy, and V.P. Dravid, *Applied Physics Letters* **111**
(14), 143106 (2017).
- 30 W. Sohn, K.C. Kwon, J.M. Suh, T.H. Lee, K.C. Roh, and H.W. Jang, *Nano Convergence* **8** (1),
11 (2021).
- 31 V.L. Nguyen, M. Seol, J. Kwon, E.-K. Lee, W.-J. Jang, H.W. Kim, C. Liang, J.H. Kang, J. Park,
M.S. Yoo, and H.-J. Shin, *Nature Electronics* **6** (2), 146 (2023).
- 32 C.J. McClellan, E. Yalon, K.K.H. Smithe, S.V. Suryavanshi, and E. Pop, *ACS Nano* **15** (1), 1587
(2021).
- 33 J.L. Doherty, S.G. Noyce, Z. Cheng, H. Abuzaid, and A.D. Franklin, *ACS Applied Materials &*
Interfaces **12** (31), 35698 (2020).
- 34 J.S. Ko, A. Shearer, S. Lee, K. Neilson, M. Jaikissoon, K. Kim, S. Bent, K. Saraswat, and E. Pop,
presented at the 2024 IEEE Symposium on VLSI Technology and Circuits (VLSI Technology
and Circuits), 2024.
- 35 C. Sheng, X. Wang, X. Dong, Y. Hu, Y. Zhu, D. Wang, S. Gou, Q. Sun, Z. Zhang, J. Zhang, M.
Ao, H. Chen, Y. Tian, J. Shang, Y. Song, X. He, Z. Xu, L. Li, P. Zhou, and W. Bao, *Advanced*
Functional Materials **34** (29), 2400008 (2024).
- 36 L. Hoang, M. Jaikissoon, Ç. Köroğlu, Z. Zhang, R.K.A. Bennett, J.-H. Song, J.A. Yang, J.-S. Ko,
M.L. Brongersma, K.C. Saraswat, E. Pop, and A.J. Mannix, *Nano Letters* **24** (41), 12768 (2024).
- 37 L. Wang, P. Makk, S. Zihlmann, A. Baumgartner, D.I. Indolese, K. Watanabe, T. Taniguchi, and
C. Schönenberger, *Physical Review Letters* **124** (15), 157701 (2020).
- 38 K.-A.N. Duerloo, Y. Li, and E.J. Reed, *Nature Communications* **5** (1), 4214 (2014).
- 39 P. Johari and V.B. Shenoy, *ACS Nano* **6** (6), 5449 (2012).
- 40 H. He, P. Lu, L. Wu, C. Zhang, Y. Song, P. Guan, and S. Wang, *Nanoscale Research Letters* **11**
(1), 330 (2016).
- 41 T.G. Ryu, H.S. Park, H.Y. Choi, S.B. Eadi, and H.D. Lee, *Materials Letters* **362**, 136193 (2024).

Supplementary Material

Direct X-Ray Measurements of Strain in Monolayer MoS₂ from Capping Layers and Geometrical Features

Kathryn Neilson¹, Marc Jaikissoon¹, Dante Zakhidov², Tara Peña¹, Alberto Salleo², Krishna Saraswat^{1,2}, and Eric Pop^{1,2,3}*

¹ Department of Electrical Engineering, Stanford University, Stanford, CA 94305

² Department of Materials Science and Engineering, Stanford University, Stanford, CA 94305

³ Department of Applied Physics, Stanford University, Stanford, CA 94305

*Contact: epop@stanford.edu

S1. Strain calculation details

X-ray diffraction spectra are fit using a Gaussian curve, centered at 2θ , representing an averaged value over the x-ray spot size. The tables below reports the films probed, their corresponding lattice spacing, and strain. MoS₂ films are measured as-grown (at 750 °C on SiO₂/Si), unless described as “transferred” (onto a new SiO₂/Si substrate). Strain percentages are calculated with respect to their preparation method, i.e. as-grown or transferred MoS₂. As-grown and transferred MoS₂ with no encapsulation layer are calculated in reference to the theoretical value. Negative strains indicate imparted compressive strain.

Table S1: Comparing as-grown and transferred MoS₂ to expected MoS₂ lattice spacing.

Film	2θ (°)	d (Å)	Strain (%)
Expected MoS ₂ ^{1,2}	18.613	2.738	
As-grown MoS ₂	18.552	2.747	0.33
Transferred MoS ₂	18.646	2.733	-0.18

Table S2: Comparing imparted strain on as-grown versus transferred MoS₂ films.

Film	2θ (°)	d (Å)	Strain (%)
As-grown MoS ₂	18.552	2.747	
Transferred MoS ₂	18.646	2.733	
MoS ₂ with Al seed + 5 nm Al ₂ O ₃ at 130 °C + 15 nm SiN _x	18.595	2.741	-0.23
Transferred MoS ₂ with Al seed + 5 nm 130 °C Al ₂ O ₃ + 15 nm SiN _x	18.646	2.733	0.00

Table S3: Comparing the imparted strain on alumina deposited at different temperatures.

Film	2θ (°)	d (Å)	Strain (%)
As-grown MoS ₂	18.552	2.747	
MoS ₂ with Al seed + 15 nm Al ₂ O ₃ at 130 °C	18.567	2.745	-0.08
MoS ₂ with Al seed + 15 nm Al ₂ O ₃ at 200 °C	18.570	2.745	-0.09
MoS ₂ with Al seed + 15 nm Al ₂ O ₃ at 300 °C	18.563	2.746	-0.06

Table S4: Comparing the effect of increasing alumina thickness on imparted strain.

Film	2θ (°)	d (Å)	Strain (%)
As-grown MoS ₂	18.552	2.747	
MoS ₂ with 1.5 nm Al seed layer	18.574	2.744	-0.12
MoS ₂ with 1.5 nm Al seed + 15 nm Al ₂ O ₃ at 130 °C	18.567	2.745	-0.08
MoS ₂ with 1.5 nm Al seed + 20 nm Al ₂ O ₃ at 130 °C	18.581	2.743	-0.15
MoS ₂ with 1.5 nm Al seed + 25 nm Al ₂ O ₃ at 130 °C	18.565	2.745	-0.07

Table S5: Comparing blanket versus patterning films and the effect of patterning on imparted strain.

Film	2θ (°)	d (Å)	Strain (%)
As-grown MoS ₂	18.552	2.747	
MoS ₂ with 1.5 nm Al seed + 15 nm Al ₂ O ₃ at 130 °C	18.567	2.745	-0.08
MoS ₂ patterned with Al seed & 15 nm ALD Al ₂ O ₃ at 130 °C	18.634	2.735	-0.44

Table S6: Evaluating the strain in a highly strained film stack with transferred MoS₂.

Film	2θ (°)	d (Å)	Strain (%)
Transferred MoS ₂	18.646	2.733	
Transferred MoS ₂ with 5 nm Au, 2.5 nm Ti, and 20 nm Ni	18.170	2.80	2.45

Table S7: Metal diffraction lattice spacings corresponding to the structure shown in **Fig. 4a**. The choice of plane and subsequent d spacing for each material is based on those closest to the measured 2θ range and the theoretical intensity of the plane.

Material	Bravais Lattice	Space Group	d (Å)	Plane	Reference
Au	Cubic	Fm-3m	2.355	(111)	3
Ti	Hexagonal	P63/mmc	2.555	(100)	4
Ni	Cubic	Fm-3m	2.034	(111)	3
Au ₂ Ti	Tetragonal	I4/mmm	2.425	(110)	5
Au ₄ Ti	Tetragonal	I4/m	2.337	(121)	6
AuTi ₃	Cubic	Pm-3n	2.549	(200)	7
AuTi	Hexagonal	P63/mmc	2.832	(100)	8
AuTi	Cubic	Pm-3m	3.250	(100)	9
Au ₃ Ti	Cubic	Pm-3n	2.550	(200)	9
Au _{0.36} TiNi _{0.64}	Cubic	Pm-3m	3.087	(100)	10
Au _{0.36} TiNi _{0.64}	Orthorhombic	Pmma	3.190	(101)	10
Au ₃ Ni	Cubic	Pm-3m	2.828	(110)	11
AuNi	Cubic	Fm-3m	2.218	(111)	12
Ni ₃ Ti	Hexagonal	P63/mmc	2.132	(201)	13
Ni ₄ Ti ₃	Hexagonal	R-3	2.128	(410)	14
NiTi	Hexagonal	P3	2.138	(11-2)	15
NiTi ₂	Cubic	Fd-3m	2.302	(422)	16
TiS ₂	Hexagonal	P-3m1	2.622	(011)	17
TiS ₃	Monoclinic	P21/m	2.902	(003)	18
MoS ₂	Hexagonal	P63/mmc	2.738	(100)	1
MoS ₂	Hexagonal	P-3m1	2.780	(100)	19
Fig. 4b, Leftmost Peak			2.894		This work

Supplementary References

- 1 R.G. Dickinson and L. Pauling, *Journal of the American Chemical Society* **45** (6), 1466 (1923).
- 2 J.A. Wilson and A.D. Yoffe, *Advances in Physics* **18** (73), 193 (1969).
- 3 H.E. Swanson and E. Tatge, *Standard X-ray diffraction powder patterns. Vol. I, Data for 54 inorganic substances*. (National Bureau of Standards, [Washington, D.C.], 1953).
- 4 D. Grier and G. McCarthy, North Dakota State University: Fargo, ND, USA (1991).
- 5 K. Schubert, M. Balk, S. Bhan, H. Breimer, P. Esslinger, and E. Stolz, *Naturwissenschaften* **46** (23), 647 (1959).
- 6 P. Pietrokowsky, *J Inst Metals* **90**, 434 (1962).
- 7 H.E. Swanson, H.F. McMurdie, M.C. Morris, and E.H. Evans, *Standard X-ray diffraction powder patterns*. (National Bureau of Standards, [Washington, D.C.], 1968).
- 8 B.-X. Liu, *physica status solidi (a)* **75** (1), K77 (1983).
- 9 P. Duwez and C.B. Jordan, *Acta Crystallographica* **5**, 213 (1952).
- 10 R. Delville, H. Shi, R.D. James, and D. Schryvers, *Solid State Phenomena* **172-174**, 105 (2011).
- 11 Y. Vasquez, Z. Luo, and R.E. Schaak, *Journal of the American Chemical Society* **130** (36), 11866 (2008).
- 12 A. Crawley and D. Fabian, *Inst Metals J* **94** (1), 39 (1966).
- 13 D.M. Poole and W. Hume-Rothery, *J. Inst. Metals* **83** (1955).
- 14 H. Sitepu, *Powder Diffraction* **24** (4), 315 (2009).
- 15 V. Krishnan, R.M. Manjeri, B. Clausen, D.W. Brown, and R. Vaidyanathan, *Materials Science and Engineering: A* **481**, 3 (2008).
- 16 G. Yurko, J. Barton, and J.G. Parr, *Acta Crystallographica* **12** (11), 909 (1959).
- 17 T. Kusawake, Y. Takahashi, and K.-I. Ohshima, *Molecular Crystals and Liquid Crystals Science and Technology. Section A. Molecular Crystals and Liquid Crystals* **341** (2), 93 (2000).
- 18 S. Furuseth, L. Brattås, and A. Kjekshus, *Acta Chemica Scandinavica* **29a**, 623 (1975).
- 19 T. Hu, R. Li, and J. Dong, *The Journal of Chemical Physics* **139** (17), 174702 (2013).